Journal of Catalysis 286 (2012) 22–29

Contents lists available at SciVerse ScienceDirect

Journal of Catalysis

journal homepage: www.elsevier.com/locate/jcat

High-resolution in situ and ex situ TEM studies on graphene formation and growth on Pt nanoparticles

Zhenmeng Peng [a], Ferenc Somodi [a], Stig Helveg [d], Christian Kisielowski [b], Petra Specht [c], Alexis T. Bell [a,*]

[a] Department of Chemical and Biomolecular Engineering, University of California, Berkeley, CA 94720, United States
[b] Joint Center for Artificial Photosynthesis, Lawrence Berkeley National Laboratory, 1 Cyclotron Road, Berkeley, CA 94720, United States
[c] Department of Materials Science and Engineering, University of California, Berkeley, CA 94720, United States
[d] Haldor Topsøe A/S, Nymøllevej 55, DK-2800 Kgs. Lyngby, Denmark

ARTICLE INFO

Article history:
Received 6 August 2011
Revised 11 October 2011
Accepted 13 October 2011
Available online 21 November 2011

Keywords:
Platinum
Nanoparticles
Graphene
In situ experiment
High-resolution electron microscopy

ABSTRACT

The formation of graphene layers on MgO-supported Pt nanoparticles was studied by both in situ and ex situ high-resolution transmission electron microscopy (HRTEM). The HRTEM images indicate that graphene sheets grow from steps in the surface of Pt nanoparticles. The subsequent morphology of the graphene sheets is a strong function of Pt particle size. For particles less than ~6 nm in diameter, the graphene sheets form nanotubes or move from the surface of Pt particles and accumulate on the MgO support. Complete particle envelopment by multiple graphene layers was only observed for particle greater than ~6 nm in diameter. The observed dependence of graphene morphology on Pt nanoparticle size and shape is associated with the strain energy generated between graphene layers during their growth and the overall free energy of the graphene-Pt system.

1. Introduction

Supported platinum nanoparticles are widely used to catalyze the transformation of alkanes via reactions such as dehydrogenation [1–4], dehydroaromatization [5,6], isomerization [7,8], and hydrogenolysis [9,10]. A by-product of these reactions is the deposition of coke, which can lead to changes in product distribution and, more importantly, to catalyst deactivation [11,12]. For these reasons, there has been an ongoing interest in finding ways to stabilize the activity of supported Pt nanoparticles and to understand the processes by which coke forms and accumulates on the surface of such particles. Good progress toward the first of these objectives has been achieved by alloying Pt with elements such as Sn, Ga, and In [3,4,13]. However, relatively little is known about the mechanism of carbon formation on Pt.

Transmission electron microscopy (TEM) has proven to be an invaluable tool in understanding the deposition of carbon on 3d transition metals (Ni, Fe, and Co) catalysts [14–22] and has been used to make deductions about the elementary processes involved. Notwithstanding the valuable information obtained from these efforts, the mechanism of carbon formation and growth continues to be the subject of intense discussion. In general, carbon atoms can be produced by the adsorption and subsequent stepwise dehydrogenation and C–C bond cleavage of hydrocarbons on the metal surfaces. The nascent carbon atoms may then diffuse from the adsorption sites to the centers for graphene growth among one of two routes. The first route involves dissolution of carbon into the bulk of the metal nanoparticles. Once the metal is saturated, carbon segregates to the metal surface where the formation of graphene initiates. The carbon formation on these metals is thus controlled by bulk solubility and diffusion of carbon atoms, as evidenced by change in lattice parameter, the formation of carbides at elevated temperatures, and kinetic studies [19–23]. The alternative perspective is that the transport of carbon is mediated by surface or sub-surface diffusion on the metal nanoparticles so the surface properties alone are sufficient to describe the graphene growth [15,24–26]. As concerns the growth centers, recent high-resolution transmission electron microscopy (HRTEM) studies indicate that these are associated with step sites in the surface of Ni and Fe/Co nanoparticles [15,17–19]. The preference for the step-mediated growth by Ni has been explained by the site-dependent adsorption energies of carbon obtained by density functional theory (DFT) [15,27].

In contrast to Ni, Fe, and Co, only a small number of TEM studies on carbon formation on Pt have been reported [28–31]. Previous work suggests that the dissolution and bulk diffusion mechanism of carbon deposition does not apply to Pt because of the very low solubility of carbon in Pt [32], and it has been proposed, therefore, that carbon deposition on Pt proceeds via a surface diffusion

* Corresponding author. Fax: +1 510 642 4778.
E-mail address: bell@cchem.berkeley.edu (A.T. Bell).

0021-9517/$ - see front matter © 2011 Elsevier Inc. All rights reserved.
doi:10.1016/j.jcat.2011.10.008

mechanism [26,33]. However, to the best of our knowledge, experimental evidence to support this transport mechanism as well as the surface processes involved in the assembly of graphene has not been presented.

The aim of the present study was to investigate the formation of graphene layers on Pt nanoparticles supported on cubic magnesium oxide (MgO). Both in situ and ex situ high-resolution TEM (HRTEM) were used for this purpose. In situ characterization of the working catalyst was undertaken in order to obtain direct observation of the formation and growth of graphene sheets under the reaction condition. These efforts were complemented by ex situ characterization of carbon deposits using HRTEM to obtain additional information about the structure of the deposited carbon. Using this approach, a systematic investigation was undertaken of the effects of Pt particle size and shape on the deposition of graphene.

2. Experimental

2.1. Synthesis of Pt nanoparticles

Platinum nanoparticles with average diameters of 3.5 and 6.1 nm were prepared by reduction of platinum acetylacetonate ($Pt(acac)_2$) dissolved in octyl ether (OE) by 1,2-hexadecanediol (HDD) in the presence of oleylamine (OAm) and oleic acid (OA). All experiments were conducted under Ar using a standard Schlenk line. To produce 3.5 nm Pt particles, platinum acetylacetonate ($Pt(acac)_2$, 97%, Aldrich, 0.05 g or 0.125 mmol) was dissolved in a mixture of OE (99%, Aldrich, 2 mL), HDD (90%, Aldrich, 0.2 g or 0.77 mmol), OAm (70%, Aldrich, 0.2 mL), and OA (99%, Aldrich, 0.2 mL) in a 25-mL three-neck flask. The resulting solution was heated to 290 °C at a rate of 5 °C/min and maintained at this temperature for 10 min before cooling down to ambient room temperatures. To make 6.1-nm Pt nanoparticles, $Pt(acac)_2$ (0.05 g or 0.125 mmol) dissolved in OE (1 mL) was injected into the organic mixture after it was heated to 290 °C [34]. A large amount of anhydrous ethanol was added to the reaction mixture to aid in the separation of Pt nanoparticles by centrifugation at 3000 rpm for 5 min. The solid material produced in this manner was dispersed in 3 mL of anhydrous toluene, forming a stable colloidal solution.

2.2. Preparation of MgO-supported Pt catalysts

MgO (<50 nm, Aldrich) was calcined in air at 1060 °C for 30 min in order to form MgO nanocubes [35]. A suspension of 0.2 g of MgO in 10 mL of anhydrous toluene was stirred under an inert atmosphere, after which an appropriate volume of the Pt suspension (containing 0.01 g Pt) was added. The mixture was stirred overnight, and the resulting product was precipitated out by adding three times the volume anhydrous ethanol. MgO-supported Pt was then separated by centrifugation. The solid material was heated at 300 °C for 1 h in air to remove the surface capping agents and then reduced in an atmosphere of H_2 in Ar (10 vol.%) at 600 °C for 1 h.

A sample of 1.4-nm-diameter Pt nanoparticles supported on MgO was prepared by incipient wetness impregnation. $Pt(acac)_2$ (0.02 g or 0.05 mmol) was dissolved in anhydrous toluene (1 mL) and added drop wisely onto the calcined MgO support (1 g) under continuous stirring. The solid was dried under vacuum and then reduced in H_2/Ar (10 vol.%) by raising the temperature to 600 °C at 5 °C/min and maintaining at 600 °C for 1 h.

2.3. In situ HRTEM

In situ TEM experiments were carried out using an image aberration-corrected Titan 80-300 ETEM microscope equipped with a differentially pumped environmental cell. The microscope was operated in TEM mode at an acceleration voltage of 300 kV, with an activated spherical aberration corrector and with an electron beam dose rate in the range of 10^4–10^6 e^-/nm^2 s incident on the CCD camera. Specimens were prepared by crushing and dispersing dry catalyst powders onto a plasma-cleaned stainless steel grid. The grid was mounted in a Gatan 628 single-tilt heading holder with an isotropic information transfer out to at least 0.14 nm. The specimens were first reduced by heating the sample in 1 mbar H_2 to 500 °C for 30–60 min, after which the sample was cooled to 475 °C. The deposition of graphene was initiated by the removal of hydrogen and introduction of 1.3 mbar isobutene. TEM images and time-lapsed TEM image series were acquired in situ of samples during the exposure to isobutene once the sample drift had leveled out, usually in less than 10 min. A low electron dose of 1.5×10^5 e^-/nm^2 s was used for in situ observations of carbon deposition in order to minimize the effects of the electron beam on the process of carbon generation and the structure of the carbon formed. For the single TEM images, the exposure time was 0.5 s. For the time series, each image was taken over a period of 0.1 s. The image series are represented with an improved signal-to-noise ratio by adding five consecutive images after making accurate alignments and appropriate indexing of the images.

2.4. Deposition of carbon for ex situ characterization

In a typical procedure, 25 mg of catalyst was loaded into a quartz tube reactor and heated to 600 °C at 15 °C/min in 20% H_2 in He using a three-zone furnace at total pressure of an atmosphere. The catalyst was maintained at this temperature for 1 h before being exposed to a mixture of ethane (C_2H_6), H_2, and He. The ratio of the volumetric flow rates of C_2H_6 and H_2 was fixed at 1:1.25, and total flow rate was maintained at 60 cm^3/min. The reaction was terminated after a fixed period of time by switching the reacting gases to pure He and cooling the sample down to room temperature. The samples were then removed from the reactor and stored in a vacuum desiccator.

2.5. Ex situ characterization by HRTEM, EELS, and Raman spectroscopy

Transmission electron microscopy (TEM) images were taken using a FEI Tecnai 12 microscope with an accelerating voltage of 120 kV. High-resolution TEM (HRTEM) characterizations were conducted on the TEAM 0.5 high-resolution microscope operated at 80 kV at the National Center for Electron Microscopy (NCEM) [36]. This instrument is a modified FEI Titan 80-300 microscope equipped with a special high-brightness Schottky field emission electron source, a gun monochromator, a high-resolution GIF Tridiem energy filter, and two CEOS (correlated electron optical systems) hexapole-type spherical aberration correctors. Scanning transmission electron microscopy (STEM) and electron energy loss spectroscopy (EELS) data were collected on a FEI Titan S80-300 microscope operated at 300 kV and under the high-angle annular dark field (HAADF) mode. Raman spectra were recorded using a Kaiser Optical HoloLab series 5000 Raman spectrometer equipped with a Nd:YAG laser source.

3. Results and discussion

Fig. 1 shows TEM images of the calcined MgO powders used to support Pt. Calcination at 1060 °C produced almost perfect cubes about 30 nm on edge. The lattice fringes are parallel to the surface of each cube and have a spacing of 2.11 Å, indicating that the MgO cubes are bounded by (200) planes (PDF 87-0652). Fig. 2a shows a TEM image of the as-synthesized Pt nanoparticles, and Fig. 2b

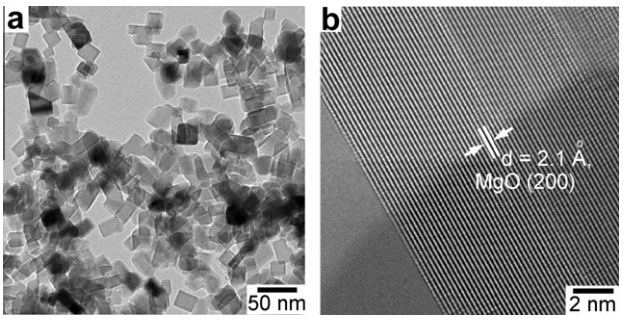

Fig. 1. (a) TEM and (b) HRTEM images of the cubic MgO support.

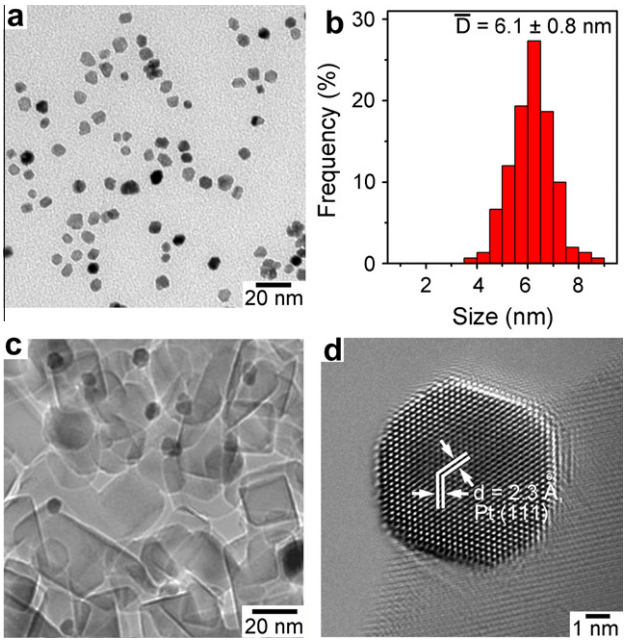

Fig. 2. (a) TEM and (b) size distribution of as-synthesized Pt nanoparticles and (c and d) TEM and HRTEM images of the supported Pt nanoparticles.

shows the distribution of Pt particle sizes. Most of the particles are uniform in size and faceted in shape. Statistical analysis of particle size distribution gives an average diameter of 6.1 ± 0.8 nm. An image of Pt nanoparticles supported on MgO is presented in Fig. 2c. It is evident that sintering of the Pt particles did not occur during calcination to remove the capping agents. The absence of sintering is attributed to the interactions of the Pt particles with the support [37]. The cubic shape of the MgO support and the low Z numbers of the Mg and O enable clear images of the Pt nanoparticles to be acquired, many of which can be observed in profile at the edges of the MgO cubes. A high-resolution image of a representative Pt particle is shown in Fig. 2d. Lattice fringes with a periodic spacing of 2.27 Å corresponding to the Pt(1 1 1) plane are clearly visible (PDF 70-2057). The observation of a straight surface with atomic resolution suggests that the organic molecules present on the particle surface after synthesis have been removed without altering the surface morphology of the particle.

In situ HRTEM observations of the Pt/MgO (d_{Pt} = 6.1 nm) catalyst were initiated by reducing the catalyst at 500 °C for 30 min in 1 mbar H_2. Fig. 3 shows representative TEM images of the supported Pt particles under the H_2 atmosphere. The image of the sample taken in situ (Fig. 3a) is very similar in appearance to that taken ex situ (Fig. 2a). Faceted particles with distinct edges were observed, suggesting a minimal effect of in situ reduction in the

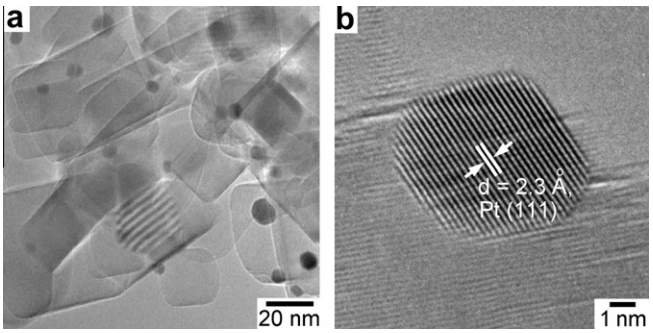

Fig. 3. In situ TEM images of supported Pt nanoparticles at (a) low and (b) high magnifications reduced in 1 mbar H_2 at 500 °C, taken with an electron dose of: (a) 5.0×10^4 and (b) 2.5×10^6 e^-/nm^2 s.

shape of the Pt nanoparticles. As in Fig. 2d, Fig. 3b shows clear evidence for (1 1 1) lattice fringes.

Carbon formation on Pt under the microscope conditions was studied by switching the composition of the gas fed to the sample holder from H_2 to a hydrocarbon. Although most light hydrocarbons are thought to form carbon on metal surfaces via a similar mechanism [14], the growth conditions can be quite different reflecting differences in the carbon chemical potential, μ_C, of the gaseous hydrocarbon. Attempts to generate a carbonaceous deposit in the microscope using 1.1 mbar ethane were unsuccessful at temperatures up to 575 °C, in contrast to ex situ experiments in which ethane was used to generate carbon deposits [38]. Equally unsuccessful attempts were made using 1.3 mbar ethene, a principal source of carbonaceous deposits used for the growth of carbon nanostructures on 3d transition metals [39]. The findings indicate that the chemical potential is too low for graphene formation at the pressure in the mbar range in the microscope. However, previous work shows that isobutene readily produced carbonaceous deposits on Pt under mild reaction conditions [40]. Accordingly, carbon deposition was indeed observed when 1.3 mbar isobutene was introduced in the microscope with the sample heated to 475 °C.

Fig. 4 presents a series of co-added images taken during the deposition of carbon on Pt/MgO. The first image (Fig. 4a) was recorded after about 10 min of exposure of the Pt particle to isobutene, whereas the next three images (Fig. 4b–d) were taken 1 s, 1.2 min, and 3.2 min after the first image. Details on the initial carbonaceous layers may be seen in Fig. S1. While evidence for the lattice fringes of Pt can be observed in Fig. 4, they are not as clearly evident as those seen in Fig. 3b. The reason for this is the greater motion of the sample occurring after the change over from H_2 to isobutene, coupled with lower signal-to-noise ratio of the heavier molecules and the slight blurring of the fringes upon the addition of sequential images taken with low electron beam exposure. The deposition of carbonaceous layers is clearly evidenced by the appearance of multiple layers growing outward from the surface of Pt particle. Fig. 4a suggests that growth of the carbonaceous layers initiates from the particle surface, most likely at the Pt steps, as indicated by the red arrows, and terminates either on the Pt surface or on the support, as indicated by the blue arrow. No changes in particle size or morphology were observed during carbon deposition, indicating that the multiple carbon layers formed without strongly affecting the compact and facetted shape of the Pt nanoparticles. The measured spacing of the graphene layers was around 3.5 Å and indexed to the (0 0 2) plane of graphite. This interlayer spacing is larger than that for well-crystallized graphitic carbon, 3.35 Å, (PDF 13-0148), suggesting that the carbonaceous deposit is turbostratic [14]. The somewhat higher interlayer spacing for the carbonaceous deposit formed in situ may also be due to graphene layers not being fully devoid of hydrogen.

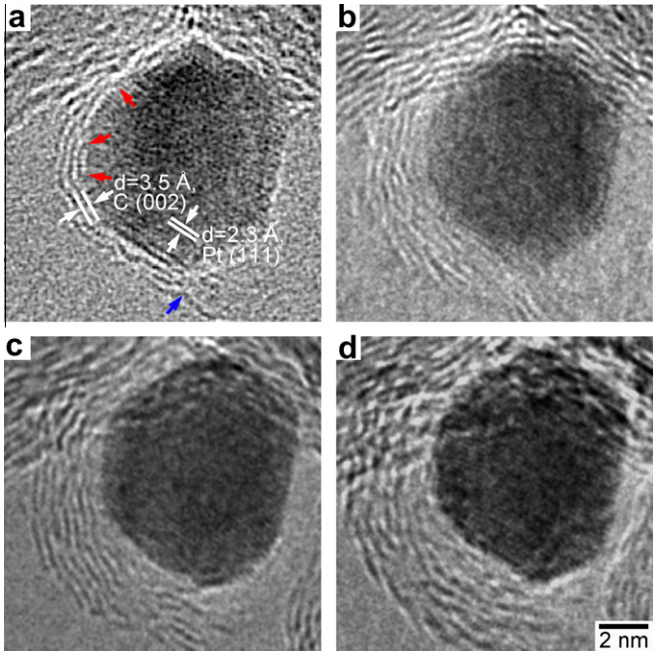

Fig. 4. Time-lapsed HRTEM images of the growing graphene layers on Pt recorded in situ under exposure of 1.3 mbar iso-butene at 475 °C (a: 0 s; b: 1 s; c: 1.2 min; and d: 3.2 min), taken with an electron dose of 1.5×10^5 e^-/nm^2 s.

The sample observed in situ under exposure to isobutene was characterized ex situ using the TEAM 0.5 microscope. A representative image is shown in Fig. 5. It should be noted that particle shown is one that had not been exposed to the effects of the electron beam during in situ studies. The carbonaceous layers seen in Fig. 5 are somewhat better ordered than those seen in Fig. 4, and the number of layers is smaller than the number seen in Fig. 4d. These differences suggest that carbon growth kinetics observed in situ was influenced by the presence of the electron beam and that further optimization of the beam dosage is needed to extract quantitative information from such time series [41].

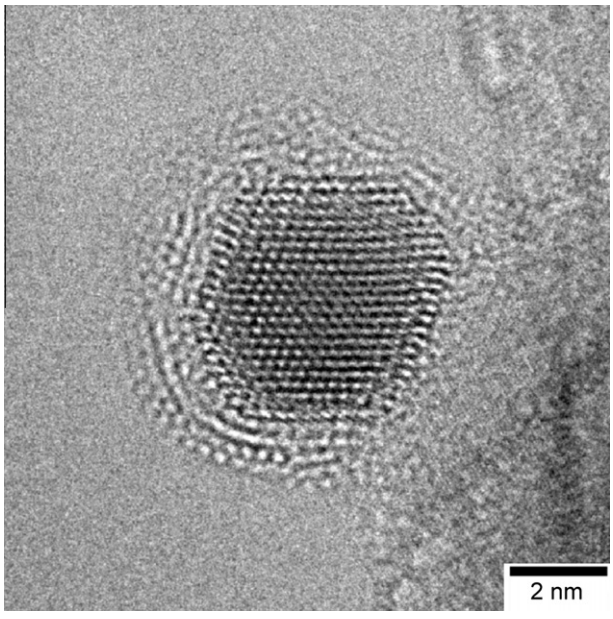

Fig. 5. Ex situ HRTEM image of the grown graphene layers on Pt after being exposed under 1.3 mbar iso-butene for 60 min at 475 °C in the in situ experiment, taken with an electron dose of 7.8×10^4 e^-/nm^2 s.

Fig. 6 shows representative ex situ HRTEM images of Pt particles observed after Pt/MgO (d_{Pt} = 6.1 nm) had been used for the dehydrogenation of ethane for 1, 2, 10, and 60 min. All Pt nanoparticles about 6 nm in diameter and larger were completely covered by layers of graphene, the number of which increased with increasing time of exposure to ethane dehydrogenation. The spacing between these layers is around 3.4 Å, consistent with that of graphite. After 1 min of exposure to the reaction mixture (Fig. 6a), two to three graphene layers were formed. The number of graphene layers grew with further time under dehydrogenation conditions, but the rate of growth between 10 and 60 min was clearly slower than upon initial exposure of the catalyst to reaction conditions. The decrease in the rate of carbon deposition is very likely due to the inhibition of atomic carbon formation on the surface of Pt nanoparticles by the accumulating layers of graphene.

Raman and EELS spectroscopy were used to confirm the attribution of the deposits seen in Fig. 6 to graphene. Raman spectra of Pt/MgO (d_{Pt} = 6.1 nm) taken after 1 min and 60 min of use for ethane dehydrogenation are shown in Fig. 7. Two broad peaks at around 1600 and 1350 cm^{-1} were observed after 1 min of reaction. The first of these features corresponds to the G band associated with the longitudinal optical (LO) phonon mode of graphite, and the second feature corresponds to the D band due to the structural disorder and the presence of carbon edges [42–44]. Both peaks increased in intensity and became better defined after 60 min of reaction, indicating a greater amount of deposited carbon. The broader shape of the G band compared to that observed for crystalline graphite suggests that defects are present among the graphene layers deposited during ethane dehydrogenation [43]. The presence of both D and G bands with comparable intensities is indicative of structural disorder in the graphene layers [44]. The slight downscale shift of the D and G bands to 1593 and 1341 cm^{-1} with increasing exposure to reaction conditions can be attributed to an increase in the number of graphene layers [43]. EELS spectra collected on individual Pt particles provide further evidence for the deposition of carbon. Fig. 8 shows the EELS K-edge region of

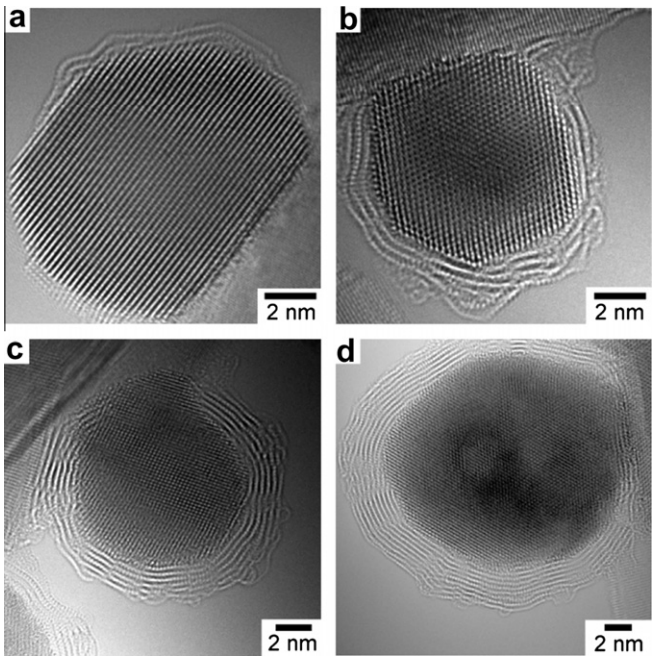

Fig. 6. HRTEM images of the graphene layers grown on Pt nanoparticles after (a) 1, (b) 2, (c) 10, and (d) 60 min of reaction at 600 °C in the forming gas, V_{C2H6}:V_{H2}:V_{He} = 12:15:33 mL/min, taken with an electron dose of around 3×10^6 e^-/nm^2 s.

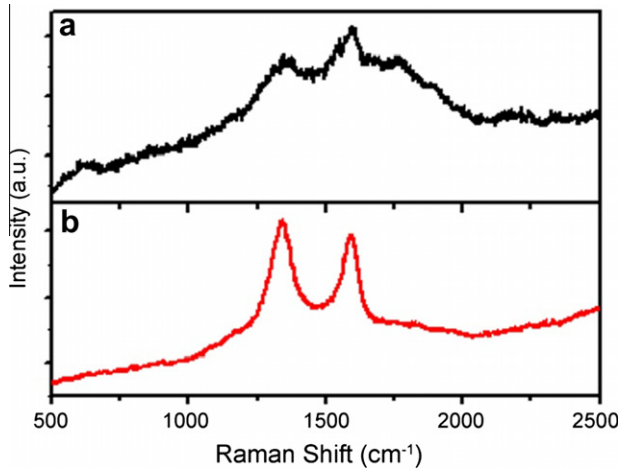

Fig. 7. Raman spectra of the worked catalyst after (a) 1 and (b) 60 min of reaction at 600 °C in the forming gas, V_{C2H6}:V_{H2}:V_{He} = 12:15:33 mL/min.

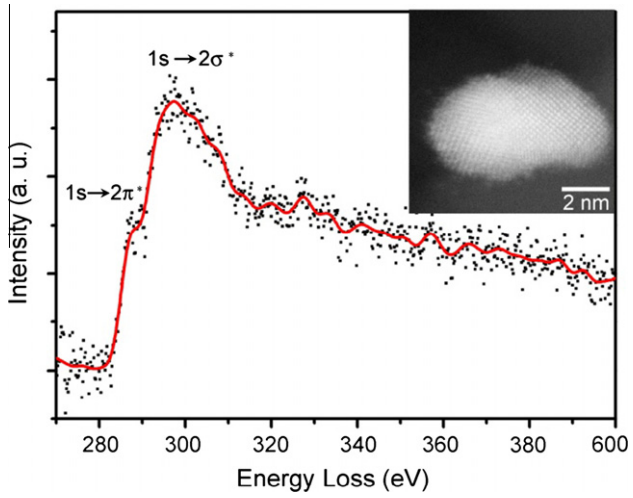

Fig. 8. EELS spectrum of one single Pt particle after 60 min of reaction at 600 °C in the forming gas, V_{C2H6}:V_{H2}:V_{He} = 12:15:33 mL/min, STEM image of the Pt particle shown in the inset.

carbon. The peak centered at around 297 eV corresponds to the transition from the 1s core level to the σ^* band and the small shoulder peak at around 288 eV can be assigned to the 1s to the π^* transition [45]. Both of these features are characteristic of graphene layers.

As noted in the discussion of Fig. 4, the formation of carbonaceous sheets appears to initiate at steps in the surface of Pt nanoparticles. Further evidence for a step-mediated growth of graphene on Pt is provided by Fig. S2 where it is seen that the first several layers of graphene bind preferentially to Pt steps. The finding that graphene grows out from Pt steps is similar to the observation of graphene growth from methane or acethylene decomposition on Ni nanoparticles [14,15,17,18]. In contrast to what was observed in those studies, the Pt particles retain their compact and facetted shape as the layers of carbon accumulate in the present experiments. However, surface restructuring was observed on some of the Pt nanoparticles as evidenced by the disappearance of clear facets and edges. These changes are probably associated with a decrease in the melting point of surface Pt and its interaction with the carbonaceous species [46,47]. Moreover, a minor fraction of the Pt particles were irregularly shaped either as a result of the synthesis or the interaction with the alkene dehydrogenation

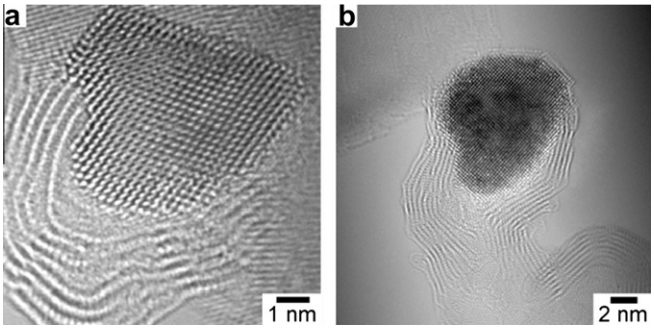

Fig. 9. HRTEM images of the grown carbon on the shaped Pt particles at the (a) early and (b) late stages, V_{C2H6}:V_{H2}:V_{He} = 12:15:33 mL/min, T = 600 °C, taken with an electron dose of around 3×10^6 e^-/nm^2 s.

environment. On such particles, carbon nanotubes (CNTs), rather than graphene shells, were observed. Fig. 9a shows a HRTEM image of one CNT in the early stage, which appears to grow from the Pt steps via a base-growth mechanism [18]. Notably, though, the tip of this Pt particle remained free of carbon throughout the growth process (see Fig. 9b). We believe that detachment of the graphene layers from the tip of the Pt particle is due to the high strain in the layers imposed by the increasing surface curvature as the tip of the particle is approached.

To further address the role of strain on the growth of graphene layers, the effect of the Pt particle size on the growth of graphene layers was examined. Fig. 10 shows images illustrating the patterns of graphene layer growth on Pt nanoparticle with diameters of around 4 and 2 nm taken after 1, 2, and 60 min of time on stream. Carbon deposition on the 4-nm particles resulted in a relative small number of graphene layers, which with time formed a capped nanotube and then grew away from the Pt particle (see Fig. 10a–c). In contrast, on the 2-nm particles, the newly formed graphene layers appear to immediately slough off onto the MgO support. Thus, the pattern of graphene layer growth on small Pt particles is distinctly different from that seen on larger (>6 nm) Pt particles, which build up an increasing number of graphene layers that envelope the particle with increasing time under reaction conditions. The different patterns of the graphene growth on Pt may help explain the observed effects of particle size on the activity, selectivity, and degree of coking of supported Pt for a number of reactions [12,48,49].

The results of this investigation clearly demonstrate that the formation of graphene on the surface of Pt nanoparticles initiates at steps in the particle surface and that the extent of graphene formation under identical reaction conditions is particle size dependent. For particles larger than ~6 nm, particles become completely enveloped in multiple layers of graphene; for particles between 6 and 2 nm, graphene nanotubules are formed, and for particles ≤2 nm, graphene layers formed on the particle surface are transported to the support. It is useful to examine these observations in light of a simple model for graphene growth at step sites on transition metal surfaces [33]. The authors of this study show based upon DFT calculations of the adsorption energies for carbon atoms that carbon atoms adsorbed on terrace surfaces are unstable to those adsorbed at step edges. For metals such as Ni and Co, the carbon adsorption energy is further decreased upon incorporation of the atom into a finite graphene layer adsorbed at the step edge. But for metals such as Ru and Rh, the transfer of a carbon atom to such a finite graphene layer is unfavorable. The origin of this difference in behavior is the strain energy, E_{strain}, resulting from epitaxial lattice mismatch between the metal step edge and graphene. This mismatch is minimal for Ni and Co but becomes substantial for Ru and Rh and is even higher for Pt. A thermodynamic model for

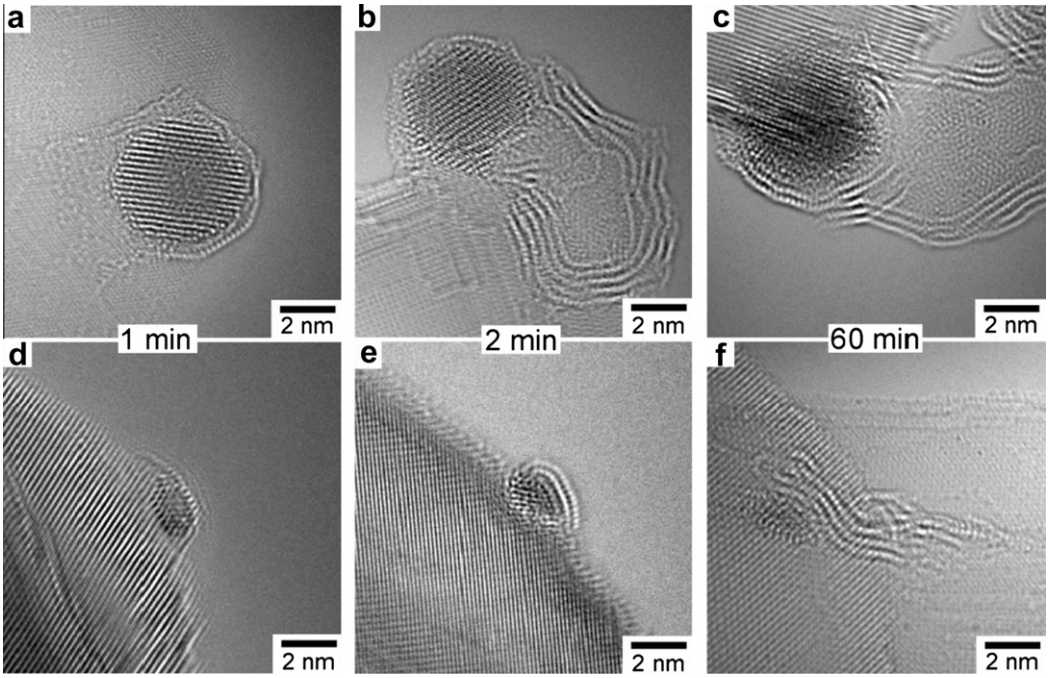

Fig. 10. HRTEM images of the grown carbon on (a–c) 3.5 and (e and f) 1.4 nm Pt nanoparticles after (a and d) 1, (b and e) 2, and (c and f) 60 min of reaction at 600 °C in the forming gas, V_{C2H6}:V_{H2}:V_{He} = 12:15:33 mL/min, taken with an electron dose of around 3×10^6 e^-/nm^2 s.

graphene growth is then developed for the purpose of identifying the critical number of carbon atoms that must be accumulated into a nascent graphene island in order to nucleate the continued growth of the sheet. The resulting expression is

$$\Delta G = -N_{tot}\Delta\mu_C + 2\sqrt{\frac{N_{tot}}{3}}E_{edge} + E_{stretch}N_{tot}, \quad (1)$$

where ΔG is the total free energy change for a semi-hexagonal graphene island; N_{tot} is the total number of atoms in the graphene island; $\Delta\mu_C$ is the carbon chemical potential, i.e., the difference in the chemical potentials of carbon in the precursor state and in graphene; E_{edge} is the energy cost per carbon atom in the perimeter of the island relative to that in an infinite graphene sheet; and $E_{stretch}$ is the cost associated with stretching the finite-sized graphene layer along the {1 0 1} zigzag direction to an epitaxial match with the step edges as a function of the total number of carbon atoms. The authors of Ref. [33] propose that $E_{stretch}$ can be estimated from the value of E_{strain}, the strain energy of an infinite graphene layer stretched (or compressed) at its edge to match the M–M distance along the zigzag {1 0 1} step of the metal. The critical value of N_{tot} above which graphene growth on a metal will be stable, N_C, is determined by letting $d\Delta G/dN_{tot} = 0$.

Application of Eq. 1 to determine N_C for Pt, assuming that the precursor for carbon deposition is C_2H_6, reveals an interesting situation. The value of $\Delta\mu_C$ at 600 °C in the present case is 0.40 eV [50], whereas the values of E_{edge} and E_{strain} are estimated to be 0.80 eV and 0.55 eV, respectively [33]. Because of the value of E_{strain} for Pt exceeds the $\Delta\mu_C$, ΔG is always positive, suggesting that the nucleation of graphene could not occur. The authors of Ref. [33] point out, however, that the assumption that $E_{stretch} \approx E_{strain}$ may overestimate the energy associated with larger, finite-sized graphene islands, because the perimeter atoms away from the step edge may have more degrees of freedom to match the metal lattice. By contrast, evidence from a number of sources indicates that graphene has only a small interaction with a Pt(1 1 1) surface and that the growth of graphene on this surface is not epitaxial [51–57]. Because of this weak interaction, stress relaxation of graphene sheets formed on Pt(1 1 1) can be relieved by the formation of folds and wrinkles. Consistent with these findings, the graphene-Pt(1 1 1) separation and the separation of two graphene sheets are found to be ≈3.30 Å, nearly identical to the interlayer spacing of graphite, 3.36 Å [51]. On the basis of this evidence, it is reasonable to conclude that $E_{stretch}$ would be considerably smaller than 0.55 eV. If it assumed that $E_{stretch}$ = 0.30 eV, the value of Ir, a metal that also exhibits a weak graphene–metal interaction [52], then N_C for Pt is estimated to be 21 and the corresponding value of N_{edge} is 5. This means that in order to nucleate a graphene layer the step edges should contain more than five Pt atoms or be about 1.4 nm (5 × 0.278 nm) in length. Consistent with these calculations, we observe that particles with average diameters smaller than about 2 nm do not form much carbon, since only a fraction of such particles will be sufficiently large to nucleate graphene growth at 600 °C. A similar effect of metal particle size on the rate of carbon deposition has been reported previously for Ni particles [27]. We note, however, that with increasing temperature the value of $\Delta\mu_C$ increases and hence the value of N_C decreases, from which it is concluded that the average size of Pt nanoparticles on which graphene formation can occur declines with increasing temperature. Moreover, as the value of $\Delta\mu_C$ becomes larger when isobutene instead of ethane is used for carbon deposition, ΔG decreased correspondingly, thereby facilitating carbon growth, in agreement with our in situ TEM observations. Similarly, if elements are alloyed with Pt, e.g., Sn, Ga, In, which cause an increase in E_{strain} or that just block the steps for carbon, then the value of N_C will increase and the temperature required to nucleate graphene growth on a Pt bimetallic particles of a given size will increase [27].

The picture of graphene formation described earlier is also consistent with the TEM images presented in Figs. 6, 9 and 10, which show the distance between the Pt particle and the first graphene and between adjacent graphene–graphene layers is ∼3.5 Å. These large distances are similar to those reported in surface science studies on graphene formation on Pt(1 1 1) [51]. Of particular note is the large spacing between graphene layers seen in Fig. 9. Further evidence of weak interaction between Pt and the graphene basal plane is the presence of numerous folds and wrinkles in the

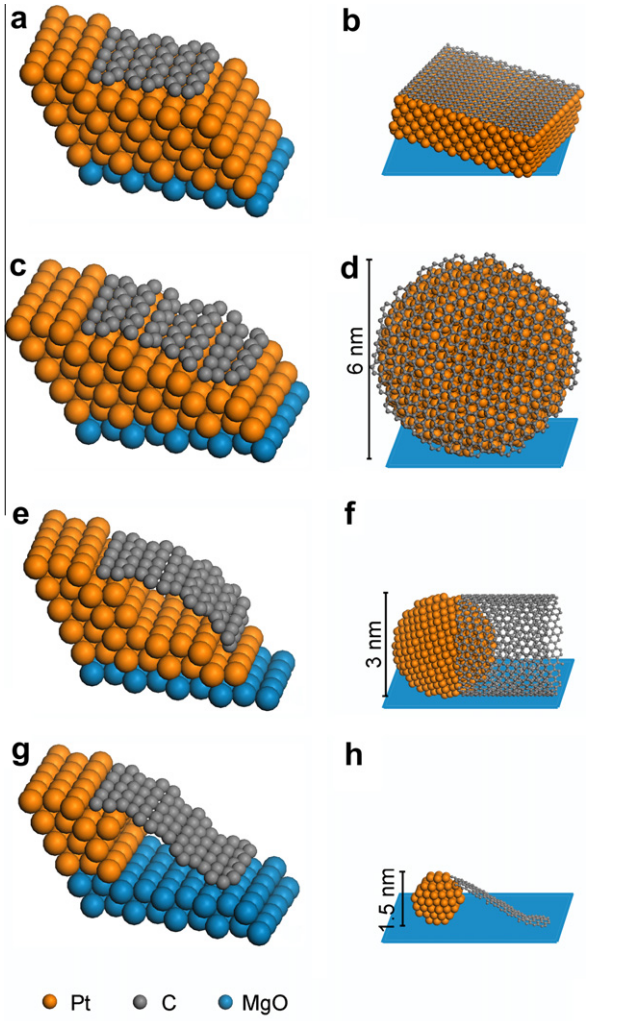

Fig. 11. Schematic illustration of graphene layer growth on Pt particles of increasing size: (a and b) graphene growth from onto the (1 1 1) surface of Pt initiated at a [1 0 1] step; (c and d) envelopment of Pt particles by graphene for particles greater than ~6 nm in diameter; (e and f) formation of graphene nanotubes on Pt particles of 2–6 nm; (g and h) formation of graphene sheets and their migration to the support for Pt particles less than 2 nm in diameter.

graphene layers after they are formed, features that can be clearly seen in Figs. 9 and 10.

The changes in the form of graphene growth with Pt particle size can be explained in terms of the balance between the free energy gained upon the formation of graphene and the interactions between graphene layers and the strain in the graphene layers induced by bending the layers so that they can contour the surface of particles on which they are formed. While interlayer interactions will work to stabilize the growth of graphene, bending of the layers will offset this stabilization. It is for this reason that the form of graphene growth is dependent on the size of the Pt nanoparticles. This point is illustrated by the schematics of graphene layer growth shown in Fig. 11.

4. Conclusions

Both in situ and ex situ HRTEM experiments were used to investigate carbon formation upon exposure of MgO-supported Pt nanoparticles to hydrocarbons. TEM observations suggest that the formation of graphene layers initiates at low-coordination number sites located at step on the surface of Pt nanoparticles. The absence of any change in the lattice parameters of Pt during the course of carbon deposition supports the proposal that carbon deposition occurs via a surface diffusion mechanism. The progress of graphene layer growth depends on both the size and shape of the Pt particles. Particles of greater than about 6 nm in diameter become enveloped in layer of turbostratic graphene, the number of which grows with the time of exposure of the sample to hydrocarbon. For smaller Pt particles, the graphene layers can form carbon nanotubes or sheets that slough off onto the support. The size dependency of carbon growth is attributed to the accommodation of strain energy generated in the graphene layers and the minimization of overall free energy in the growth process. Pt particles of similar size but varied shape catalyzed the formation of different carbon structures under the same condition, revealing other contributing factors besides the traditional understanding on their growth. The systematic study on size and shape effects on the carbon deposition may be instructive in developing new catalyst intended for both carbon growth and suppression. In particular, we suggest that the observed suppression of carbon deposition on bimetallic Pt nanoparticles containing Sn, Ga, or In as the second element may be due to the presence of these elements at the edges of step in the metal particles, where they may inhibit the nucleation of graphene layer growth.

Acknowledgments

The authors express their appreciation for the opportunity to obtain in situ HRTEM images at Haldor Topsøe A/S and to Sven Ullmann for his contribution to this effort. This work was supported by a grant from Chevron Energy Technology Company. The authors acknowledge support of the National Center for Electron Microscopy, Lawrence Berkeley Lab, which is supported by the US Department of Energy under Contract DE-AC02-05CH11231.

Appendix A. Supplementary material

Supplementary data associated with this article can be found, in the online version, at doi:10.1016/j.jcat.2011.10.008.

References

[1] D.J. Trevor, R.L. Whetten, D.M. Cox, A. Kaldor, J. Am. Chem. Soc. 107 (1985) 518–519.
[2] S. Vajda, M.J. Pellin, J.P. Greeley, C.L. Marshall, L.A. Curtiss, G.A. Ballentine, J.W. Elam, S. Catillon-Mucherie, P.C. Redfern, F. Mehmood, P. Zapol, Nat. Mater. 8 (2009) 213–216.
[3] V. Galvita, G. Siddiqi, P.P. Sun, A.T. Bell, J. Catal. 271 (2010) 209–219.
[4] G. Siddiqi, P.P. Sun, V. Galvita, A.T. Bell, J. Catal. 274 (2010) 200–206.
[5] R.J. Davis, E.G. Derouane, Nature 349 (1991) 313–315.
[6] Z. Paal, P. Tetenyi, J. Catal. 30 (1973) 350–361.
[7] Y. Barron, D. Cornet, G. Maire, F.G. Gault, J. Catal. 2 (1963) 152–155.
[8] I. Lee, F. Zaera, J. Am. Chem. Soc. 127 (2005) 12174–12175.
[9] Y. Barron, G. Maire, J.M. Muller, F.G. Gault, J. Catal. 5 (1966) 428–445.
[10] R.D. Cortright, R.M. Watwe, J.A. Dumesic, J. Mol. Catal. A – Chem. 163 (2000) 91–103.
[11] G.F. Froment, Catal. Rev.-Sci. Eng. 50 (2008) 1–18.
[12] Z. Paal, A. Wootsch, R. Schlogl, U. Wild, Appl. Catal. A – Gen. 282 (2005) 135–145.
[13] F. Humblot, J.P. Candy, F. Le Peltier, B. Didillon, J.M. Basset, J. Catal. 179 (1998) 459–468.
[14] K.P. De Jong, J.W. Geus, Catal. Rev.-Sci. Eng. 42 (2000) 481–510.
[15] S. Helveg, C. Lopez-Cartes, J. Sehested, P.L. Hansen, B.S. Clausen, J.R. Rostrup-Nielsen, F. Abild-Pedersen, J.K. Nørskov, Nature 427 (2004) 426–429.
[16] A.T. Bell, Nature 456 (2008) 185–186.
[17] S. Hofmann, R. Sharma, C. Ducati, G. Du, C. Mattevi, C. Cepek, M. Cantoro, S. Pisana, A. Parvez, F. Cervantes-Sodi, A.C. Ferrari, R. Dunin-Borkowski, S. Lizzit, L. Petaccia, A. Goldoni, J. Robertson, Nano Lett. 7 (2007) 602–608.
[18] M. Lin, J.P.Y. Tan, C. Boothroyd, K.P. Loh, E.S. Tok, Y.L. Foo, Nano Lett. 6 (2006) 449–452.
[19] J.A. Rodriguez-Manzo, M. Terrones, H. Terrones, H.W. Kroto, L.T. Sun, F. Banhart, Nat. Nanotechnol. 2 (2007) 307–311.
[20] R.T.K. Baker, P.S. Harris, R.B. Thomas, R.J. Waite, J. Catal. 30 (1973) 86–95.
[21] R. Sharma, E. Moore, P. Rez, M.M.J. Treacy, Nano Lett. 9 (2009) 689–694.

[22] H. Yoshida, S. Takeda, T. Uchiyama, H. Kohno, Y. Homma, Nano Lett. 8 (2008) 2082–2086.
[23] R.T.K. Baker, M.A. Barber, P.S. Harris, F.S. Feates, R.J. Waite, J. Catal. 26 (1972) 51–62.
[24] F. Abild-Pedersen, J.K. Nørskov, J.R. Rostrup-Nielsen, J. Sehested, S. Helveg, Phys. Rev. B 73 (2006) 115419.
[25] O.V. Yazyev, A. Pasquarello, Phys. Rev. Lett. 100 (2008) 156102.
[26] S. Hofmann, G. Csanyi, A.C. Ferrari, M.C. Payne, J. Robertson, Phys. Rev. Lett. 95 (2005) 036101.
[27] H.S. Bengaard, J.K. Nørskov, J. Sehested, B.S. Clausen, L.P. Nielsen, A.M. Molenbroek, J.R. Rostrup-Nielsen, J. Catal. 209 (2002) 365–384.
[28] W.T. Owens, N.M. Rodriguez, R.T.K. Baker, J. Phys. Chem. 96 (1992) 5048–5053.
[29] N.M. Rodriguez, P.E. Anderson, A. Wootsch, U. Wild, R. Schlogl, Z. Paal, J. Catal. 197 (2001) 365–377.
[30] R.A. Cabrol, A. Oberlin, J. Catal. 89 (1984) 256–266.
[31] T.S. Chang, N.M. Rodriguez, R.T.K. Baker, J. Catal. 123 (1990) 486–495.
[32] B.J. Kang, J.H. Mun, C.Y. Hwang, B.J. Cho, J. Appl. Phys. 106 (2009) 104309.
[33] S. Saadi, F. Abild-Pedersen, S. Helveg, J. Sehested, B. Hinnemann, C.C. Appel, J.K. Nørskov, J. Phys. Chem. C 114 (2010) 11221–11227.
[34] X.W. Teng, D. Black, N.J. Watkins, Y.L. Gao, H. Yang, Nano Lett. 3 (2003) 261–264.
[35] K. Itatani, K. Koizumi, F.S. Howell, A. Kishioka, M. Kinoshita, J. Mater. Sci. 23 (1988) 3405–3412.
[36] C. Kisielowski, B. Freitag, M. Bischoff, H. van Lin, S. Lazar, G. Knippels, P. Tiemeijer, M. van der Stam, S. von Harrach, M. Stekelenburg, M. Haider, S. Uhlemann, H. Muller, P. Hartel, B. Kabius, D. Miller, I. Petrov, E.A. Olson, T. Donchev, E.A. Kenik, A.R. Lupini, J. Bentley, S.J. Pennycook, I.M. Anderson, A.M. Minor, A.K. Schmid, T. Duden, V. Radmilovic, Q.M. Ramasse, M. Watanabe, R. Erni, E.A. Stach, P. Denes, U. Dahmen, Microsc. Microanal. 14 (2008) 469–477.
[37] J.K.A. Clarke, M.J. Bradley, L.A.J. Garvie, A.J. Craven, T. Baird, J. Catal. 143 (1993) 122–137.
[38] R.S. Vincent, R.P. Lindstedt, N.A. Malik, I.A.B. Reid, B.E. Messenger, J. Catal. 260 (2008) 37–64.
[39] K. Takehira, T. Ohi, T. Shishido, T. Kawabata, K. Takaki, Appl. Catal. A – Gen. 283 (2005) 137–145.
[40] P.S. Cremer, X.C. Su, Y.R. Shen, G. Somorjai, J. Chem. Soc.-Faraday Trans. 92 (1996) 4717–4722.
[41] S.B. Simonsen, I. Chorkendorff, S. Dahl, M. Skoglundh, J. Sehested, S. Helveg, J. Am. Chem. Soc. 132 (2010) 7968–7975.
[42] M.S. Dresselhaus, A. Jorio, R. Saito, Annu. Rev. Condens. Matter Phys. 1 (2010) 89–108.
[43] A.C. Ferrari, Solid State Commun. 143 (2007) 47–57.
[44] L.M. Malard, M.A. Pimenta, G. Dresselhaus, M.S. Dresselhaus, Phys. Rep.-Rev. Sec. Phys. Lett. 473 (2009) 51–87.
[45] S. Tomita, M. Fujii, S. Hayashi, K. Yamamoto, Chem. Phys. Lett. 305 (1999) 225–229.
[46] S. Horch, H.T. Lorensen, S. Helveg, E. Laegsgaard, I. Stensgaard, K.W. Jacobsen, J.K. Nørskov, F. Besenbacher, Nature 398 (1999) 134–136.
[47] E.C. Garnett, W.J. Liang, P.D. Yang, Adv. Mater. 19 (2007) 2946–2950.
[48] M.S. Kumar, D. Chen, J.C. Walmsley, A. Holmen, Catal. Commun. 9 (2008) 747–750.
[49] R.M. Rioux, H. Song, J.D. Hoefelmeyer, P. Yang, G.A. Somorjai, J. Phys. Chem. B 109 (2005) 2192–2202.
[50] A.B. Preobrajenski, M.L. Ng, A.S. Vinogradov, N. Martensson, Phys. Rev. B 78 (2008) 073401.
[51] P. Sutter, J.T. Sadowski, E. Sutter, Phys. Rev. B 80 (2009) 245411.
[52] J. Coraux, A.T. N'Diaye, M. Engler, C. Busse, D. Wall, N. Buckanie, F. Heringdorf, R. van Gastel, B. Poelsema, T. Michely, New J. Phys. 11 (2009) 023006.
[53] D.E. Starr, E.M. Pazhetnov, A.I. Stadnichenko, A.I. Boronin, S.K. Shaikhutdinov, Surf. Sci. 600 (2006) 2688–2695.
[54] M. Sasaki, Y. Yamada, Y. Ogiwara, S. Yagyu, S. Yamamoto, Phys. Rev. B 61 (2000) 15653–15656.
[55] M. Enachescu, D. Schleef, D.F. Ogletree, M. Salmeron, Phys. Rev. B 60 (1999) 16913–16919.
[56] T.A. Land, T. Michely, R.J. Behm, J.C. Hemminger, G. Comsa, Surf. Sci. 264 (1992) 261–270.
[57] Z.P. Hu, D.F. Ogletree, M.A. Vanhove, G.A. Somorjai, Surf. Sci. 180 (1987) 433–459.